

Contents

2	1 Diamond detectors for radiation detection	2
3	1.1 Semiconductor detectors	3
4	1.2 Principles of signal formation in semiconductors	4
5	1.2.1 Signal induction by moving charges	6
6	1.2.2 Shockley-Ramo theorem	7
7	1.2.3 Thermal excitation and p-n junctions	8
8	1.2.4 Space charge	8
9	1.3 Carrier transport in a diamond sensor	9
10	1.4 Radiation-induced current signals	10
11	1.4.1 Mean energy loss	12
12	1.4.2 Signal fluctuation	12
13	1.4.3 Charge trapping	13
14	1.4.4 Charge collection efficiency and distance	14
15	1.5 Radiation damage	15
16	1.6 Electronics for signal processing	16
17	1.6.1 Signal preamplifiers	16
18	1.6.2 Analogue-to-digital converters	19
19	1.6.3 Digital signal processing	20

²⁰ **Chapter 1**

²¹ **Diamond detectors for radiation
²² detection**

²³ Diamond has been known for over two millennia, valued for its mechanical properties
²⁴ and its appearance. When the procedures for its synthesis were discovered, diamond
²⁵ made its way to a broad range of industries which exploit its optical and electri-
²⁶ cal properties. The discovery of the Chemical Vapour Deposition (CVD, described
²⁷ below) as a new synthesis process gave rise to a range of new applications. Purer
²⁸ specimens are used in electronics, high-power switching devices, electrochemical sys-
²⁹ tems, radiation sensors, quantum computing etc. Recently it was found that it also
³⁰ exhibits superconductivity []. This thesis focuses on the use of diamond for radiation
³¹ detection. An example of such a diamond sample is shown in figure 1.1.

³² Compared to a natural diamond, a CVD diamond used as a particle detector has
³³ almost no impurities (foreign atoms like nitrogen or boron). If proper procedures are
³⁴ followed, the diamond lattice can be grown very uniformly. This in turn improves
³⁵ electrical properties of the grown sample. Such a diamond is an almost perfect thermal
³⁶ and electrical insulator. However, its electrical behaviour is similar to that of a
³⁷ semiconductor. For this reason this chapter first introduces semiconductor detectors
³⁸ and then describes the principle of signal formation in semiconductors. Then it focuses
³⁹ on the diamond sensor and its properties.

⁴⁰ **Chemical vapour deposition** (CVD) [] is a process where a material is deposited
⁴¹ from a gas onto a substrate, involving chemical reactions. It is often carried out
⁴² under high pressure and high temperatures. It takes place in enclosed chambers
⁴³ called furnaces with careful regulation of the temperature, pressure and gas mixture.
⁴⁴ Synthetic diamond is grown at 700–900 °C with a mixture of hydrogen and methane
⁴⁵ gas. At this temperature the molecules dissociate into carbon and hydrogen atoms.
⁴⁶ The carbon atoms are the building blocks and are deposited on the surface of the
⁴⁷ substrate.
⁴⁸ Under a carefully controlled pressure and temperature conditions with an added abra-
⁴⁹ sive atomic hydrogen the graphitic bonds break and form into diamond bonds. The
⁵⁰ speed of the growth can be anywhere between 0.1 and 10 µm per hour. The detector

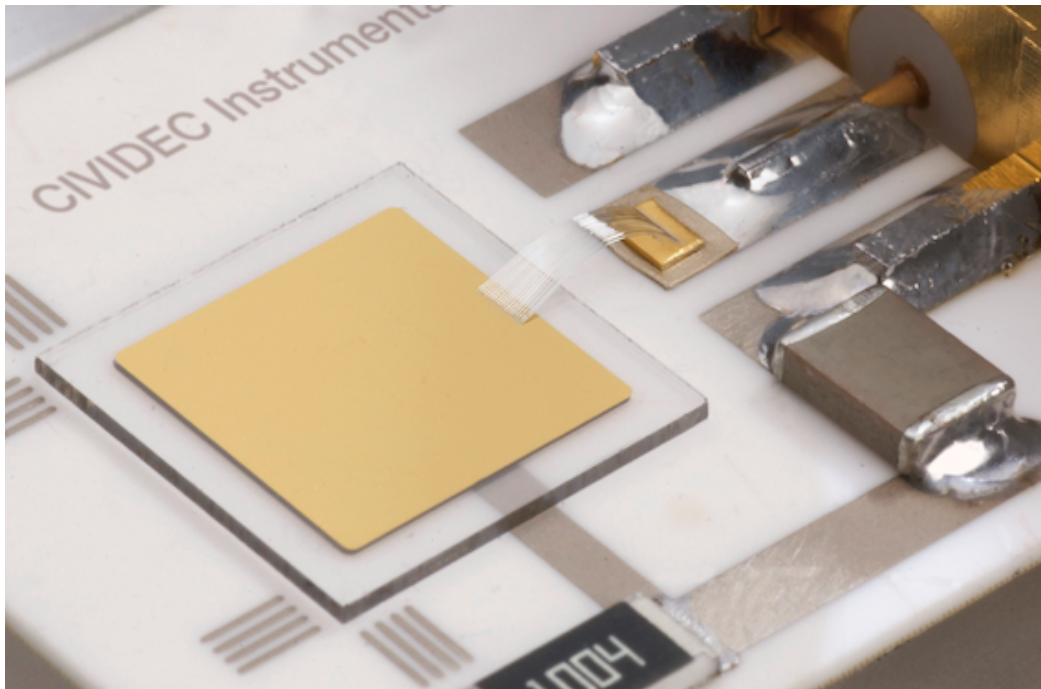


Figure 1.1: A pCVD diamond pad detector [?].

51 grade samples are grown at a rate of the order of $1 \mu\text{m}$ per hour. They can grow up to
52 several millimetres in thickness. The width of the samples, however, depends entirely
53 on the substrate used. Diamond can be deposited on various materials: diamond,
54 silicon, tungsten, quartz glass etc. The substrate material must be able to withstand
55 the high temperatures during the CVD process. The diamond substrate does not
56 need any surface pre-treatment. Carbon atoms form bonds with atoms in the exist-
57 ing crystal structure. This is the homo-epitaxial growth where the newly deposited
58 atoms retain the orientation of the structure in the substrate. Other non-diamond
59 substrates, however, need to be pre-treated, usually by being polished using diamond
60 powder. Some powder particles remain on the surface, acting as seeds for the growth
61 of small crystals or grains. These grains grow and at some point merge with the
62 adjacent ones, making up a compact material. The lower side is later polished away.
63 These diamonds are called *polycrystalline* (pCVD) whereas those grown on a diamond
64 substrate are *single crystal* (sCVD) diamonds. The area of the former can be large -
65 up to 0.5 m^2 or more compact 75 cm^2 in the case of detector grade diamonds, which
66 can be further cut into smaller parts. The sCVD diamonds, on the other hand, can
67 currently only achieve sizes up to 1.5 cm^2 .

68 1.1 Semiconductor detectors

69 Semiconductor is a class of solids whose electrical conductivity is between that of
70 a conductor and that of an insulator – of the order of $10^{-5} \Omega^{-1} \text{ cm}^{-1}$. Semicon-
71 ductors consist of atoms with four electrons in their valence band, e.g. silicon–Si or

1.2. PRINCIPLES OF SIGNAL FORMATION IN SEMICONDUCTORS

72 germanium–Ge, or as combinations of two or more different materials, e.g. gallium
73 arsenide–GaAs). The atoms in the lattice form valence bonds with adjacent atoms,
74 creating solid crystal structures.

75 Semiconductor particle detectors are devices that use a semiconductor material to
76 detect radiation. They work on the principle of an ionisation chamber. An incident
77 particle ionises the atoms in the crystal lattice. The charges are freed if the deposited
78 energy is higher than the energy band gap, i.e. the energy needed to excite an electron
79 from its steady state to the conductance band. The freed charge carriers start drifting
80 in an externally applied electric field, inducing current on the electrodes. The induced
81 signal is amplified and read out by the electronics in the detector signal chain.

82 Semiconductor detectors are most widely used for tracking applications, like the
83 Insertable B-Layer shown in figure 1.2 [?], which was installed in ATLAS Experiment
84 in 2014. First, they can be produced in thin layers to minimise the impact on the path
85 of the incident particles. Second, their low sensor capacitance allows for a fast signal
86 response. Third, they are highly efficient and highly resistant to radiation damage.
87 Finally, the industrial processes allow for a fine spatial segmentation, which in turn
88 improves the track resolution of the detector systems.

89 Semiconductor sensors come in several configurations. The simplest type is a pad
90 – a single plate with two electrodes. Pads are used for particle counting and radiation
91 monitoring. Next is a strip detector, a more finely segmented detector made out of
92 long parallel sensing areas or strips. Normally each strip has its own signal line for
93 readout. Usually the strip detectors are used in pairs – one detector is placed on top
94 of the other at an angle to increase spatial resolution in both axes. The third and
95 the most finely segmented is a pixel detector, consisting of a 2D array of independent
96 sensing areas. In tracking applications, pixel detectors are used where the need for a
97 high detection resolution and granularity requirement is the highest. Due to their high
98 production cost and a high number of signal channels, they can only cover limited
99 areas. Strip detectors can be used to cover larger areas in several consecutive layers.

100 1.2 Principles of signal formation in semiconduc- 101 tors

102 Particles can interact with the sensor in several ways, e.g. via bremsstrahlung [],
103 elastic or inelastic scattering or nuclear reactions []. Bremsstrahlung is radiation
104 created when a particle is decelerated due to interaction with the electric field of the
105 core of an atom. Elastic scattering is deflection of the particle’s trajectory due to
106 the pull from the nucleus without depositing any energy in it. This is in principle
107 an unwanted effect in semiconductors as it deteriorates the spatial resolution of the
108 sensor. Inelastic scattering is the interaction through which an electron in the atom
109 is *ionised*. Nuclear reaction is the direct interaction between the incident particle
110 and the core of the atom. All these effects are competing and are dependent on the
111 particle’s mass, momentum etc. The scope of this chapter is to discuss the ionisation



Figure 1.2: The Insertable B-Layer – a silicon particle tracker installed in the ATLAS experiment in 2014 [?].

112 mechanism in semiconductors.

113 The energy of the electrons forming valence bonds between atoms in the crystal
114 lattice is within the *valence band* []. To break a bond and excite the electron into a
115 *conduction band*, a sufficient energy has to be applied. The minimal energy required
116 is equal to the energy band gap E_g of the semiconductor. Typical E_g values are
117 0.7 eV in Ge, 1.12 eV in Si and 1.4 eV in GaAs. Diamond with its 5.5 eV band gap
118 is considered an insulator. The separation between the conductive and valence band
119 is referred to as *forbidden gap* where no electron states can exist.

120 An electron excited into the conduction band leaves behind a positively charged
121 ion with a vacancy – a hole – in its valence band, as shown in figure 1.3a. A free
122 *electron-hole pair* is thus created. The free electron travels through the crystal until
123 it is recombined with another hole. Similarly the positive charge of the hole attracts a
124 bound electron in the vicinity, causing it to break from the current bond and moving
125 to the vacancy, thus leaving behind a newly created hole. The process continues,
126 making it look like the hole is traveling through the material [].

127 Both the electron and the hole are referred to as *charge carriers*. Without an
128 externally applied electrical field, they propagate in random directions. Therefore on
129 average there is no overall motion of charge carriers in any particular direction over
130 time.

131 However, if an external electric field is applied to the crystalline structure, the free
132 electrons and holes drift toward the positive and negative potential, respectively, as
133 shown in figure 1.3b. While drifting, the charges couple with the electrodes, inducing

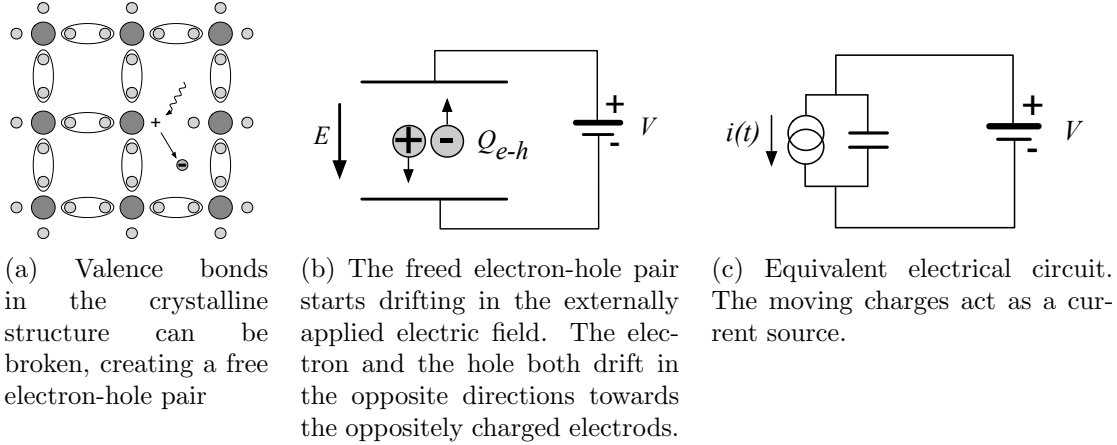


Figure 1.3: In the equivalent electrical circuit diagram the electron-hole creation and drift can be modelled as a current source with a capacitor in parallel.

¹³⁴ current in the circuit, which is explained by the Shockley–Ramo theorem below.

¹³⁵ Upon reaching the electrodes the charges stop inducing the current. The equivalent
¹³⁶ electrical circuit is shown in figure 1.3c.

¹³⁷ 1.2.1 Signal induction by moving charges

¹³⁸ The signal induction in a conducting plane by a point-like charge, which couples with
¹³⁹ an electrode, is derived in [2]. The electrode can in this case be modelled as an infinite
¹⁴⁰ conducting plane. When a point charge q is created (e.g. an electron-hole pair created
¹⁴¹ via ionisation), its electrostatic field lines immediately couple with the electrode, as
¹⁴² seen in figure 1.4a. The electric field on the metal surface due to a point-like charge
¹⁴³ q at the distance z_0 is

$$E_z(x, y) = \frac{q z_0}{2\pi\epsilon_0(x^2 + y^2 + z_0^2)^{\frac{3}{2}}} \quad E_y = E_z = 0. \quad (1.1)$$

¹⁴⁴ A mirror charge appears on the conducting plane, with a charge density distribution

$$\sigma(x, y) = \epsilon_0 E_z(x, y) = \frac{q z_0}{2\pi(x^2 + y^2 + z_0^2)^{\frac{3}{2}}}. \quad (1.2)$$

¹⁴⁵ The charge density integrated over the entire plane yields a mirror charge Q , which
¹⁴⁶ is an opposite of point charge q :

$$Q = \int_{-\infty}^{\infty} \int_{-\infty}^{\infty} \sigma(x, y) dx dy = -q. \quad (1.3)$$

¹⁴⁷ The plane is then segmented into infinitely long strips with a width w whereby each
¹⁴⁸ of the strips is grounded, as shown in figure 1.4c. Considering a charge density

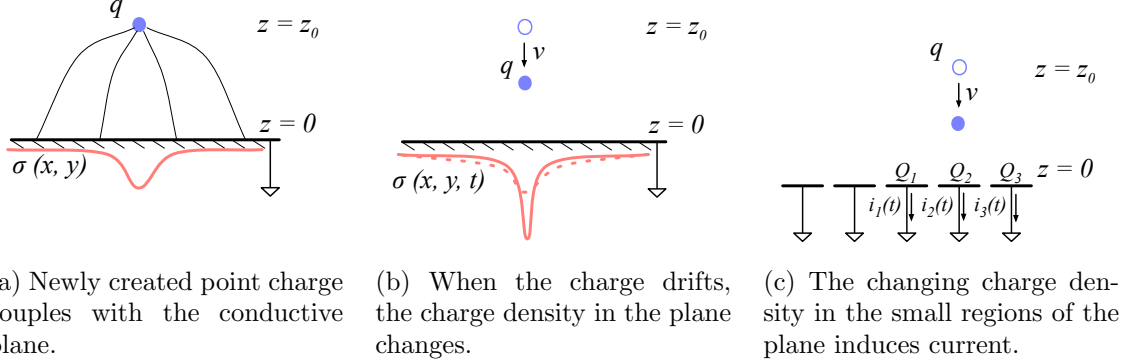


Figure 1.4: A point-like charge inducing current in a conductive plane.

¹⁴⁹ distribution 1.2, the resulting mirror charge on a single strip Q_2 directly below the
¹⁵⁰ point charge ($x = 0, y = 0$) yields

$$Q_2(z_0) = \int_{-\infty}^{\infty} \int_{-w/2}^{w/2} \sigma(x, y) dx dy = -\frac{2q}{\pi} \arctan\left(\frac{w}{2z_0}\right) \quad (1.4)$$

¹⁵¹ If the charge starts moving towards the conducting plane, the mirror charge density
¹⁵² distribution also changes, as shown in figure 1.4b. As a result the $Q_2[z(t)]$ changes
¹⁵³ with time. The changing charge is in effect an induced electric current $i_2(t)$:

$$i_2(t) = -\frac{d}{dt} Q_2[z(t)] = -\frac{\partial Q_2[z(t)]}{\partial z} \frac{\partial z(t)}{\partial t} = \frac{4qw}{\pi[4z(t)^2 + w^2]} v. \quad (1.5)$$

¹⁵⁴ The movement of the point-like charge therefore induces current in the conducting
¹⁵⁵ plane. The induced current is linearly dependent on the velocity of the point-like
¹⁵⁶ charge.

¹⁵⁷ 1.2.2 Shockley-Ramo theorem

¹⁵⁸ W. Shockley [6] and S. Ramo [5] independently proposed a theory which explains
¹⁵⁹ how a moving point charge induces current in a conductor. The Shockley-Ramo
¹⁶⁰ theorem can therefore be used to calculate the instantaneous electric current induced
¹⁶¹ by the charge carrier or a group of charge carriers. It can be used for any number of
¹⁶² electrodes. It states that the current $I_n^{\text{ind}}(t)$ induced on the grounded electrode n by
¹⁶³ a point charge q moving along a trajectory $\mathbf{x}(t)$ reads

$$I_n^{\text{ind}}(t) = -\frac{dQ_n(t)}{dt} = -\frac{q}{V_w} \nabla \Psi_n[\mathbf{x}(t)] v(t) = -\frac{q}{V_w} \mathbf{E}_n[\mathbf{x}(t)] v(t), \quad (1.6)$$

¹⁶⁴ where $\mathbf{E}_n(\mathbf{x})$ is the *weighting field* of electrode n in the case where the charge q is
¹⁶⁵ removed, electrode n is set to voltage $V_w = 1$ and all other electrodes are grounded.
¹⁶⁶ The weighting field is defined as the spatial differential of the *weighting potential*:

¹⁶⁷ $\mathbf{E}_n(\mathbf{x}) = \nabla\Psi_n(\mathbf{x})$. In the case of two parallel electrodes, the weighting field is $E_w =$
¹⁶⁸ $-\frac{d\Psi}{dx} = -1/d$, where d is the distance between the electrodes. The resulting induced
¹⁶⁹ current is therefore

$$i(t) = \frac{q}{d}v_{\text{drift}}(x, t), \quad (1.7)$$

¹⁷⁰ whereby v_{drift} is the drift velocity of the point-like charge and d is the distance between
¹⁷¹ the electrodes. d is defined by the dimensions of the sensor. The drift velocity is a
¹⁷² function of the externally applied electric field, as defined in section 1.3. If the
¹⁷³ electric field is set to a constant value, the induced current is directly proportional to
¹⁷⁴ the drifting charge. Therefore, by measuring the height of the induced current at a
¹⁷⁵ specific point of time the number of moving charges can be deduced.

¹⁷⁶ 1.2.3 Thermal excitation and p-n junctions

¹⁷⁷ Electrons can be thermally excited to the conduction band. The intrinsic concentra-
¹⁷⁸ tion of thermally excited electrons n_i in semiconductors is given as

$$n_i = T^{3/2} \cdot \exp\left(-\frac{E_g}{2k_B T}\right) \quad (1.8)$$

¹⁷⁹ wherein $k_B = 1.381 \times 10^{-23} \text{ m}^2 \text{ kg s}^{-2} \text{ K}^{-1}$ is the Boltzmann constant, E_g is the
¹⁸⁰ energy band gap of the semiconductor and T is the temperature in K. The n_i of
¹⁸¹ silicon is To reduce this effect the semiconductor sensors are doped with donors and
¹⁸² acceptors, forming a diode, The diode is then inversely biased to deplete the material
¹⁸³ of all moving charges. Doped silicon fulfils most of the needs for particle physics
¹⁸⁴ requirements and is therefore the most widely used material for particle detection.

¹⁸⁵ Due to the small band gap in semiconductors a significant amount of electrons
¹⁸⁶ already occupies the conduction band at room temperature due to thermal excitation,
¹⁸⁷ according to the probabilistic distribution.

¹⁸⁸ 1.2.4 Space charge

¹⁸⁹ The Poisson equation shows that

$$\frac{d^2\Phi(x)}{dx^2} = \frac{dE(x)}{dx} = \frac{\rho(x)}{\epsilon} \quad (1.9)$$

¹⁹⁰ where $\rho(x)$ is the space charge distribution, E is the electrical field and Φ is the
¹⁹¹ voltage potential. In an ideal diamond, the externally applied high voltage potential
¹⁹² on the two electrodes decreases linearly through the sensor. The electrical field is
¹⁹³ therefore constant throughout the sensor and the space charge distribution across it
¹⁹⁴ equals 0. However, space charge may be introduced in the material either by means of
¹⁹⁵ accumulating of charge carriers in the lattice (i.e. charge trapping) or already during
¹⁹⁶ sensor production. The space charge can be either permanent or changing – sometimes
¹⁹⁷ it is possible to reduce it, as is shown in chapter ???. All in all, it is very important to
¹⁹⁸ reduce it because it affects the shape of the electrical signal. Since the drift velocity

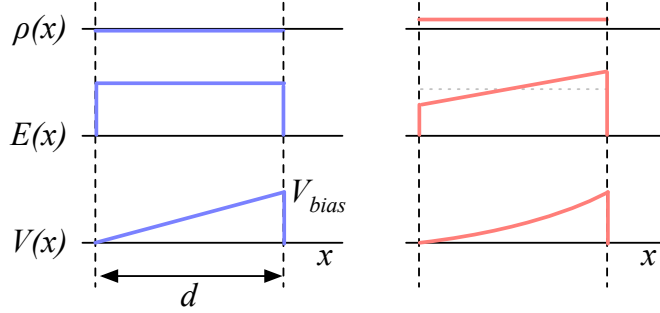


Figure 1.5: Left figure shows a profile of a diamond sensor only with an externally applied electric field. In the figure on the right a uniformly distributed space charge is added in the diamond, contributing to the internal electric field distribution. The induced current signal is proportional to the electrical field. d is the thickness of the diamond sensor.

of the charge carriers is proportional to the electrical field, the charges change their velocity while drifting through the space charge region. Figure 1.5 compares the voltage potential, the electrical field and the space charge for an ideal sensor as well as for that with a uniformly distributed positive space charge.

1.3 Carrier transport in a diamond sensor

This section describes the carrier transport phenomena in diamond. This theory provides the basis for discussion about the measurements in chapter ??.

Table 1.1 compares the properties of diamond and silicon. Some of these values are revisited and used in the course of this thesis.

Property	Diamond	Silicon
Band gap energy E_g (eV)	5.5	1.12
Electron mobility μ_e ($\text{cm}^2 \text{ V}^{-1} \text{ s}^{-1}$)	1800	1350
Hole mobility μ_h ($\text{cm}^2 \text{ V}^{-1} \text{ s}^{-1}$)	1200	450
Breakdown field (V cm^{-1})	10^7	3×10^5
Resistivity ($\Omega \text{ cm}$)	$> 10^{11}$	2.3×10^5
Intrinsic carrier density (cm^{-3})	$< 10^3$	1.5×10^{10}
Mass density (g cm^{-3})	3.52	2.33
Atomic charge	6	14
Dielectric constant ϵ	5.7	11.9
Displacement energy (eV/atom)	43	13 – 20
Energy to create an e-h pair (eV)	13	3.6
Radiation length (cm)	12.2	9.6
Avg. signal created/ μm (e)	36	89

Table 1.1: Comparison diamond – silicon [?, ?].

When the charge carriers are freed in a semiconductor with no concentration gradient and without an externally applied electric field, they scatter in random

1.4. RADIATION-INDUCED CURRENT SIGNALS

212 directions with a thermal velocity v_{th} [2]. Their integral movement due to thermal
213 excitation equals zero.

214 **Diffusion** is caused by the concentration gradient. In its presence the integral move-
215 ment is in the direction of the lower concentration until an equilibrium is reached.
216 The concentration profile dissolves with time forming a Gaussian distribution with
217 variance $\sigma(t) = \sqrt{Dt}$ [2].

218 **Drift** is caused by an externally applied electrical field. In that case the carriers move
219 along the field lines. In a sensor with a high applied field the diffusion contribution
220 is negligible.

221 **Drift velocity** $v_{\text{drift}}(E)$ is the speed at which the charge carriers drift through the
222 diamond sensor [2].

223 **Mobility** μ is a proportionality factor between the v_{drift} and the electric field E at
224 low electric fields: $v_{\text{drift}} = \mu E$. Its units are in $\text{cm}^2 \text{V}^{-1} \text{s}^{-1}$.

225 **Phonon transport** is the transfer of energy of the moving charges to the lattice.

226 **Saturation velocity** v_{sat}^e is a velocity limit above which the carriers cannot reach.
227 This is due to increasing phonon transport at a high electric field. The $v_{\text{sat}}^e = v_{\text{sat}}^h =$
228 $(14.23 \pm 0.12) \times 10^6 \text{ cm/s}$ for both positive and negative charge carriers has been
229 derived from the measurements in [4].

230 The final equation for v_{drift} is therefore

$$v_{\text{drift}}(E) = \mu(E)E = \frac{\mu_0 E}{1 + \frac{\mu_0 E}{v_{\text{sat}}}}. \quad (1.10)$$

231 It can be retrieved experimentally via the transit time measured with the Transient
232 Current Technique (TCT). This technique enables the measurement of transit time
233 t_t of the carriers through the sensor with the thickness d .

$$v_{\text{drift}}(E) = \frac{d}{t_t(E)}. \quad (1.11)$$

234 The velocities for holes and electrons usually differ. In diamond, the holes travel 30 %
235 faster than electrons [2], which is empirically confirmed in chapter ??.

236 1.4 Radiation-induced current signals

237 When a highly-energetic particle travels through the sensor, it interacts with atoms
238 in the lattice. It ionises the valence electrons, creating electron-hole (e-h) pairs on its
239 way. It can either deposit only a fraction of its energy and exit the sensor on the other
240 side or it can get stopped in the sensor, depositing all of its energy. A special case is

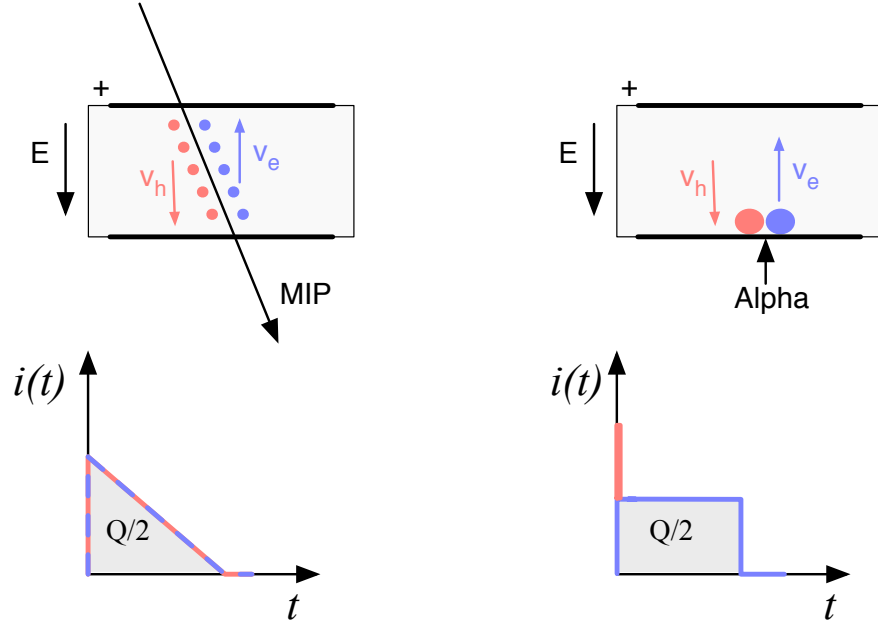


Figure 1.6: Charge carrier drift in diamond for β/γ and for α particles crossing the sensor at $t = 0$.

when it interacts with the core of the atom in the middle of the sensor by means of a nuclear interaction. All these various types interactions produce different amounts and different spatial distributions of e-h pairs.

The two most frequent types are shown in figure 1.6. The first figure shows the interaction of an incident MIP. The electrons and holes created all along the trajectory of the particle immediately start drifting towards the positive and negative electrode, respectively. At $t = 0$ all charges drift, contributing to the maximum induced current. Those closest to the electrodes have a very short drift path. They stop inducing current upon reaching the electrode. The resulting current signal is a triangular pulse with a sharp rising edge and a linear falling edge. Gradually all the charge carriers reach the electrode. The accumulated charge Q_s equals to the sum of the contributions of the positive and negative charge carriers.

The second type of interaction happens when the particle is stopped in the diamond close to the point of entry. Most of its energy is deposited in a small volume close to the electrode. A cloud of charge carriers is created and the charges with the shorter path to the electrode disappear almost instantly. The carriers of the opposite charge, however, start drifting through the sensor to the other electrode. In an ideal diamond sensor, their velocity is constant throughout the drift up until they are collected at the opposite electrode. The contribution of the first charge cloud is a peak with a short time. The cloud drifting through the sensor, on the other hand, induces a current signal with a flat top. The resulting signal has a shape of a rectangle, with a

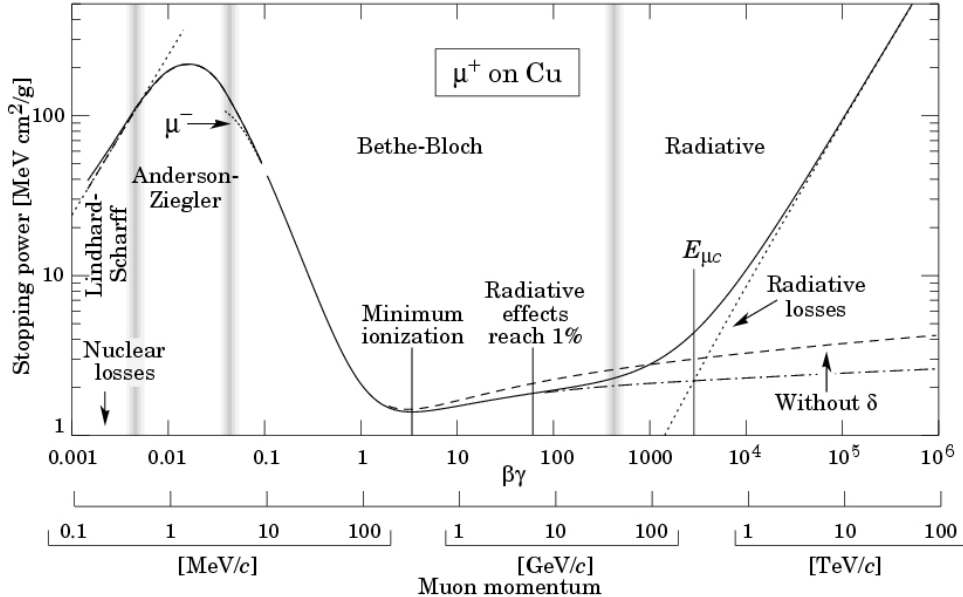


Figure 1.7: Stopping power for muons according to the Bethe-Bloch formula [].

spike in the beginning. The accumulated charge Q_s is equal to a half of the deposited charge by the stopped particle.

The two aforementioned types of interactions have well defined signal responses. Nuclear interactions on the other hand yield various results. The resulting signal shape depends on the decay products of the interaction, which can be α , β or γ quanta or other nuclei, inducing a mixed shaped signal.

1.4.1 Mean energy loss

A mean energy loss of a particle traversing the detector as a function of the momentum is given with the the Bethe-Bloch equation []:

$$-\left\langle \frac{dE}{dx} \right\rangle = \frac{4\pi}{m_e c^2} \cdot \frac{n z^2}{\beta^2} \cdot \left(\frac{e^2}{4\pi\epsilon_0} \right)^2 \cdot \left(\ln \left(\frac{2m_e c^2 \beta^2}{I \cdot (1 - \beta^2)} \right) - \beta^2 \right) \quad (1.12)$$

The resulting function for a muon is shown in figure 1.7. At a momentum of around 300 MeV/c the incident particle deposits the lowest amount of energy. Hence it is referred to as the *minimum ionising particle* or a MIP.

1.4.2 Signal fluctuation

Two important sensor properties are the magnitude of the signal and the fluctuations of the signal at a given absorbed energy. They determine the relative resolution $\Delta E/E$. For semiconductors the signal fluctuations are smaller than the simple statistical standard deviation $\sigma_Q = \sqrt{N_Q}$. Here N_Q is the number of released charge

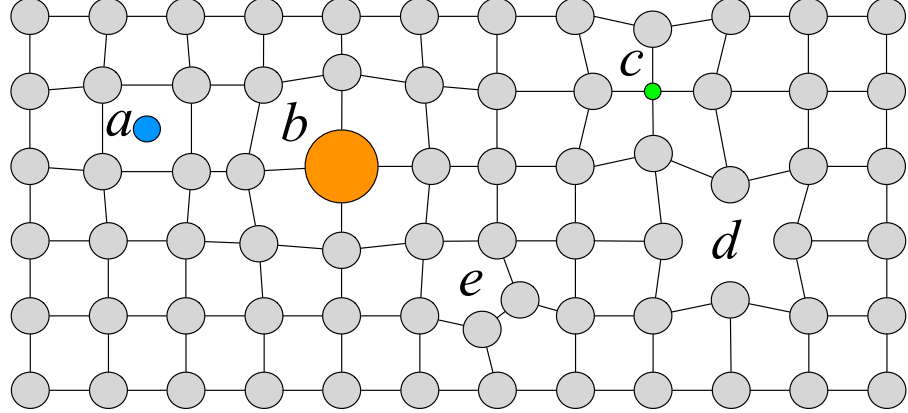


Figure 1.8: Impurities and non-uniformities in the crystal lattice due to radiation damage.

pairs, i.e. the ratio between the total deposited energy E_0 and the average energy deposition E_i required to produce an electron-hole pair. [] shows that the standard deviation is $\sigma_Q = \sqrt{FN_Q}$, where F is the Fano factor [] (0.08 for diamond and 0.115 for silicon []). Thus, the standard deviation of the signal charge is smaller than expected, $\sigma_Q \approx 0.3\sqrt{N_Q}$. The resulting intrinsic resolution of semiconductor detectors is

$$\Delta E_{\text{FWHM}} = 2.35\sqrt{FEE_i} \quad (1.13)$$

wherein $E_i(\text{Si}) = 3.6 \text{ eV}$ and $E_i(\text{Di}) = 13 \text{ eV}$. E.g., for an α particle with energy $E_\alpha = 5.486 \text{ MeV}$ the calculated resolution in diamond is equal to $\Delta E_{\text{FWHM}} = 5.6 \text{ keV}$. This defines the minimum achievable resolution for energy spectroscopy with semiconductors.

1.4.3 Charge trapping

Various types of lattice defects can be created in diamond, similar to those in silicon [?]. Figure 1.8 shows several examples of lattice damage:

- a) foreign interstitial (e.g. H, Li),
- b, c) foreign substitutional (e.g. N, P, B),
- d) vacancy and
- e) self interstitial.

These non-uniformities form new energy levels in the forbidden gap. These intermediate levels are referred to as charge traps because they can trap moving charge carriers. The energy level of the trapped carriers is reduced from the conduction band to the energy level of the trap. Different types of lattice damage have different energy

1.4. RADIATION-INDUCED CURRENT SIGNALS

300 levels. The carriers trapped in a shallow trap – an energy level close to the conduction
301 band – have a high probability of being thermally excited back into the conduction
302 band whereby they continue drifting towards the electrode. Their activation energy
303 is therefore low. Those trapped in a deep trap close to the middle of the forbidden
304 gap need a much higher activation energy, which in turn increases the average time
305 to their release due to thermal excitation.

306 The energy band jumping goes the other way, too. The carriers in the valence
307 band may use the intermediate energy levels as “stepping stones” to jump to the
308 conduction band and start drifting in the externally applied electric field. These
309 intermediate energy levels are referred to as the generation centres of leakage current.

310 1.4.4 Charge collection efficiency and distance

311 The total measured charge Q_i is the integral of the induced current:

$$Q_i = \int i_{\text{ind}}(t) dt. \quad (1.14)$$

312 The expected charge Q_0 can be calculated using the thickness of the sensor d and the
313 average number of e-h pairs created per μm δ_d , which is 36 for diamond according to
314 table 1.1. The charge collection efficiency (CCE) is the ratio between the measured
315 and expected charge:

$$CCE = \frac{Q_i}{Q_0} = \frac{Q_i}{\delta_d \cdot d} \cdot 100\%. \quad (1.15)$$

316 The charge collection distance (CCD) is a measure of an average path that the charge
317 carriers travel before getting trapped:

$$CCD = \frac{Q_i}{\delta_d} \quad (1.16)$$

318 and is usually given in units of μm .

319 Carriers that get trapped stop contributing to the overall induced current on
320 the electrodes. The more charges are trapped along their drift path, the more the
321 current induced on the electrodes is decreased. This in turn yields a lower integrated
322 charge. An expected CCE for non-irradiated sCVD diamonds is close to 100 %
323 and for non-irradiated pCVD diamonds ranges between 40 % and 60 %. In other
324 words, high-quality pCVD diamonds already have traps introduced by means of grain
325 boundaries, which are created in the growing process. Traps can also be created by
326 damaging the diamond using radiation (discussed in section 1.5). The more the sensor
327 is irradiated, the larger number of traps is introduced in the material and the higher
328 is the probability that the carriers are stopped on the way, reducing in turn the
329 integrated charge. Therefore the CCD and CCE can be used as a means to quantify
330 the detector damage due to radiation.

³³¹ 1.5 Radiation damage

³³² Exposure to ionising radiation degrades sensors by deforming the crystal lattice and
³³³ introducing charge traps in the material.

³³⁴ Radiation damage varies with the type of radiation and its energy. There are
³³⁵ several models existing [?, ?] that try to explain the impact of irradiation and to
³³⁶ provide *damage factors* to compare the radiation damage between different particles.
³³⁷ The standard way is to convert the damage into *1 MeV neutron equivalent fluence* [?].
³³⁸ Some models have been extensively verified with simulations and with experiments.
³³⁹ In these experiments the charge collection in sensors is measured before and after
³⁴⁰ irradiation. This procedure is repeated several times, with a measurement point
³⁴¹ taken after every irradiation. Then the charge collection for this set of measurements
³⁴² is plotted as a function of the radiation dose received by a specific particle at a specific
³⁴³ energy. From this a damage factor k_λ can be extracted. Damage factors have to be
³⁴⁴ measured across a range of energies and types of radiation to properly quantify the
³⁴⁵ damage in the sensors. Finally they are compared to the simulations to validate the
³⁴⁶ theoretical models.

³⁴⁷ Diamond is an expensive material and the technology is relatively new as com-
³⁴⁸ pared to silicon. Therefore few institutes are carrying out diamond irradiation studies.
³⁴⁹ To join the efforts, the RD42 collaboration [?] has been formed. It gathers the exper-
³⁵⁰imental data from diamond irradiation studies. Unlike with silicon, the experimental
³⁵¹ results so far show no significant correlation with the NIEL (non-ionising energy loss)
³⁵² model [?], which correlates detector efficiency with the number of lattice displace-
³⁵³ments. Therefore an alternative model was proposed [?], correlating the diamond
³⁵⁴ efficiency with the number of displacements per atom (DPA) in the material. The
³⁵⁵ idea is that if the recoil energy of an incident particle is higher than the lattice binding
³⁵⁶ energy (42 eV for diamond), the atom is displaced from its original position. The
³⁵⁷ newly formed vacancy acts as a trap for drifting charge carriers. The more displace-
³⁵⁸ments that form in the crystal, the higher is the probability that a drifting carrier gets
³⁵⁹ trapped. However, different types of particles interact differently with the material.
³⁶⁰ In addition the mechanisms of interaction at low energies are different to those at
³⁶¹ high energies. To assess the damage for individual particles at a range of energies,
³⁶² simulations need to be run first. The simulation shown in [?] shows the DPA model
³⁶³ for a range of energies of proton, pion and neutron irradiation in diamond. Figure 1.9
³⁶⁴ contains the simulation results as well as the superimposed empirical results of several
³⁶⁵ irradiation studies. According to the figure, a 300 MeV pion beam damages the dia-
³⁶⁶mond material twice as much as a 24 GeV proton beam. The data points obtained by
³⁶⁷ RD42 are also added to the figure. They have been normalised to damage by 24 GeV
³⁶⁸ protons.

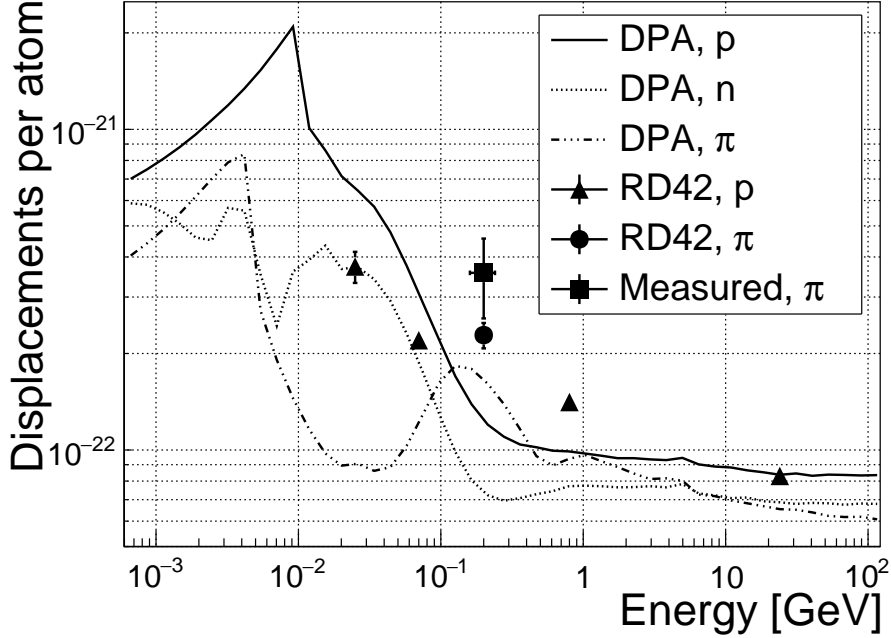


Figure 1.9: Diamond radiation damage - a model based on displacements per atom [?]. The figure shows the DPA as a function of the kinetic energy for protons, neutrons and pions. Added are data points for protons and pions by RD42 [?].

369 1.6 Temperature effects

370 1.7 Electronics for signal processing

371 This section describes the electronics of a detector, starting with a description of
372 signal amplifiers and then discussing the digitisation and signal processing. All these
373 stages are necessary to extract information from the sensor. First, the signal has to be
374 amplified. Then it is digitised and finally processed in a specially designed processor
375 or a logic unit.

376 1.7.1 Signal preamplifiers

377 The signal charge generated in the sensor by a single energetic particle is of the order
378 of fC. The induced current range is typically between 10^{-8} A (β, γ radiation) and
379 3×10^{-7} A (α radiation). Signals as low as these have to be pre-amplified before
380 processing. Depending on the measurement, several types of signal amplifiers can be
381 used. The preamplifiers are designed to minimise electronic noise while maximising
382 gain, thus maximising the signal-to-noise ratio (SNR). In addition, a high bandwidth
383 limit is preferred to minimise the information loss due to signal shape deformation.
384 A critical parameter is the total capacitance, i.e. the sensor capacitance together
385 with the input capacitance of the preamplifier. The SNR improves with a lower

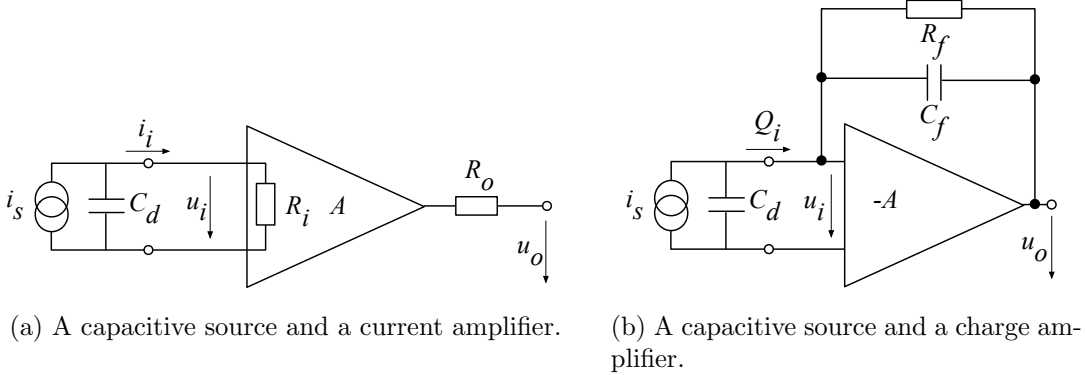


Figure 1.10: Simplified equivalent circuits of a current and charge amplifier.

386 capacitance. Several types of amplifiers can be used, all of which affect the measured
 387 pulse shape. Two preamplifiers are used most commonly, a current and a charge
 388 sensitive amplifier. Both are described in detail below.

389 Current-sensitive amplifier

390 Figure 1.10a shows the equivalent circuit of a capacitive source and a current amplifier.
 391 An amplifier operates in current mode if the source has a low charge collection
 392 time t_c with respect to the $R_i C_d$ time constant of the circuit. In this case the sensor
 393 capacitance discharges rapidly and the output current i_o is proportional to the in-
 394 stantaneous current i_i . The amplifier is providing a voltage gain, so the output signal
 395 voltage u_o is directly proportional to the input voltage u_i :

$$u_o(t) = A \cdot R_i \cdot i_s(t). \quad (1.17)$$

396 The detector capacitance C_{det} together with the input resistance of the amplifier R_i
 397 defines the time constant of the signal, as shown in figure 1.11. The higher the C_{det} ,
 398 the slower is the response of the amplifier. For the case of the diamond sensor, which
 399 has the capacitance of the order of 2 pF and the input resistance of 50 Ω, the resulting
 400 time constant is $\tau = 10^{-10}$ s. This yields the signal rise time $t_r \sim 2.2\tau = 2.2 \times 10^{-10}$ s.

401

402 Charge-sensitive amplifier

403 In order to measure integrated charge in the sensor, a feedback loop is added to the
 404 amplifier, as shown in figure 1.10b. The feedback can be used to control the gain and
 405 input resistance, as well as to integrate the input signal. The charge amplifier is in
 406 principle an inverting voltage amplifier with a high input resistance.

407 In an ideal amplifier the output voltage u_o equals $-Au_i$. Therefore the voltage
 408 difference across the capacitor C_f is $u_f = (A + 1)u_i$ and the charge deposited on the
 409 capacitor is $Q_f = C_f u_f = C_f(A + 1)u_i$. Since no current can flow into the amplifier,
 410 all of the signal current must charge up the feedback capacitance, so $Q_f = Q_i$.

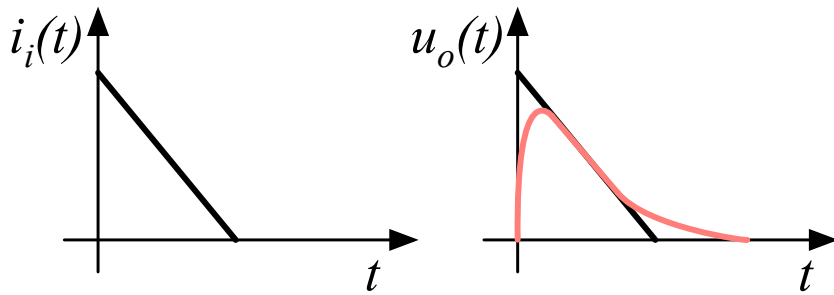


Figure 1.11: Input and output signal of the current amplifier.

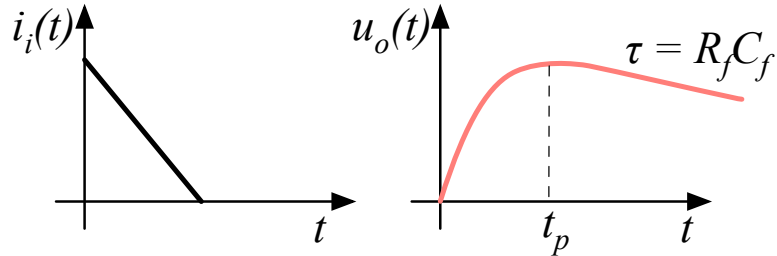


Figure 1.12: Input and output signal of the charge amplifier.

411 In reality, however, charge-sensitive amplifiers respond much slower than is the
 412 duration of the current pulse from the sensor. In addition, a resistor is added to the
 413 feedback line in parallel to the capacitor. The resistor and capacitor define the decay
 414 time constant of the pulse, as shown in figure 1.12. This is necessary to return the
 415 signal to its initial state to be ready for a new measurement.

416 **Analogue electronic noise**

417 The electronic noise determines the ability of a system to distinguish different signal
 418 levels. The analogue signal contains ample information about the type and energy
 419 of incident radiation, which can quickly be erased or altered if the signal properties
 420 change. Therefore the noise contributions to the signal must be well understood
 421 to qualify the information the signal is carrying. The important contributions are
 422 listed below. Thermal or Johnson–Nyquist [1] noise is the dominant noise contribution
 423 in the use case for diamond detector signal amplification and therefore defines the
 424 limitations of the detector system. This noise type is generated by the random thermal
 425 motion of charge carriers. The frequency range of the thermal noise is from 0 to ∞
 426 with a predominantly uniform distribution. Therefore this is nearly a white noise.
 427 The resulting signal amplitude has a Gaussian distribution. The RMS of the noise

⁴²⁸ amplitude is defined as

$$u_{\text{RMS}} = \sqrt{4k_B RT \Delta f} \quad (1.18)$$

⁴²⁹ where k_B is the Boltzmann constant, R is the input resistance of the amplifier, T its
⁴³⁰ temperature and Δf the frequency range. This equation shows that it is possible to
⁴³¹ reduce the noise RMS by either (1) reducing the frequency range, (2) reducing the
⁴³² resistance of the conductor or (3) cooling the conductor.

⁴³³ Contributions of shot noise, flicker noise and burst noise and other types are not
⁴³⁴ significant relative to the thermal noise. However, the contributions of external factors
⁴³⁵ can severely deteriorate the signal. This means the noise produced by capacitive or
⁴³⁶ inductive coupling with an external source, which causes interference in the signal.
⁴³⁷ These effects can be reduced by shielding the electronics and avoiding ground loops.

⁴³⁸ 1.7.2 Analogue-to-digital converters

⁴³⁹ An analogue-to-digital converter (ADC) is a device that converts the analogue elec-
⁴⁴⁰ trical signal on the input to its digital representation - a series of digital values. This
⁴⁴¹ involves a quantisation – *sampling* of the signal at a defined sampling period, resulting
⁴⁴² in a sequence of samples at a discrete time period and with discrete amplitude values.
⁴⁴³ The resolution of the ADC is the number of output levels the ADC can quantise to
⁴⁴⁴ and is expressed in bits. For instance, an ADC with a resolution equal to $n = 8$ bit
⁴⁴⁵ has a dynamic range of $N = 2^n = 256$ steps. The resulting voltage resolution Q_{ADC}
⁴⁴⁶ at the input voltage range of $V_{\text{ADC}} = \pm 50$ mV is then

$$Q_{\text{ADC}} = \frac{V_{\text{ADC}}}{2^n} = \frac{100 \text{ mV}}{2^8 \text{ bit}} = 0.39 \text{ mV/bit.} \quad (1.19)$$

⁴⁴⁷ With a sampling period of $t_s = 1$ ns the sampling rate is $f_s = 1$ GS/s (gigasample per
⁴⁴⁸ second).

Quantisation error and quantisation noise (or a round-off error) is a contribu-
⁴⁴⁹ tion to the overall measurement error due to digitisation (rounding). The quantisation
⁴⁵⁰ error is defined as a difference between the actual analog value and the closest digi-
⁴⁵¹ tised representation of this value, therefore by the least significant bit (LSB), as seen
⁴⁵² in figure 1.13. The input signal amplitude is typically much larger than than the
⁴⁵³ voltage resolution. In this case the quantisation error is not directly correlated with
⁴⁵⁴ the signal and has an approximately uniform distribution $[\cdot]$. The probability density
⁴⁵⁵ function $P(x)$ therefore has a rectangular shape bounded by $(-\frac{1}{2}\text{LSB}, \frac{1}{2}\text{LSB})$:

$$P(x) = \begin{cases} \frac{1}{\text{LSB}}, & -\frac{1}{2}\text{LSB} \leq x \leq \frac{1}{2}\text{LSB} \\ 0, & \text{otherwise.} \end{cases} \quad (1.20)$$

⁴⁴⁹ The height equal to $\frac{1}{\text{LSB}}$ preserves the integrated probability of 1. The variance of
⁴⁵⁰ the distribution is

$$\sigma^2 = \int P(x)(x - \mu)^2 dx. \quad (1.22)$$

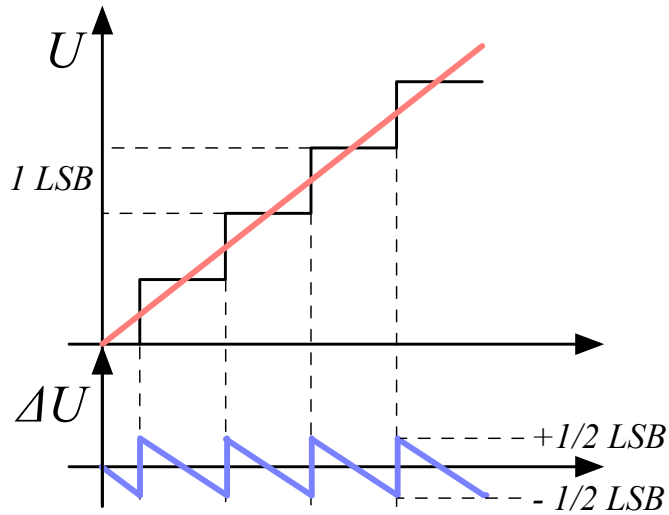


Figure 1.13: Input signal digitisation and quantisation error.

⁴⁵¹ The population mean is $\mu = 0$, therefore

$$\sigma^2 = \int_{-\frac{1}{2}\text{LSB}}^{\frac{1}{2}\text{LSB}} \frac{1}{\text{LSB}} x^2 dx = \frac{x^3}{3\text{LSB}} \Big|_{-\frac{1}{2}\text{LSB}}^{\frac{1}{2}\text{LSB}} = \frac{\text{LSB}^2}{12}. \quad (1.23)$$

⁴⁵² The RMS of the quantisation noise is defined as the square root of the variance:

$$\Delta Q_{\text{ADC}} = \sqrt{\sigma^2} = \frac{1}{\sqrt{12}} \text{LSB} \sim 0.289 \text{ LSB}. \quad (1.24)$$

⁴⁵³ For the example above the quantisation error equals $\Delta Q_{\text{ADC}} = 0.289 \cdot 0.39 \text{ mV} = 0.11 \text{ mV}$. The error depends strongly on the linearity of the ADC, but this is out of scope of this document as the devices used have ADCs with a very good linearity.

⁴⁵⁶ 1.7.3 Digital signal processing

⁴⁵⁷ The digitised signal can be processed to extract useful information. Therefore after ⁴⁵⁸ the signal amplification and digitisation the signal is routed in a device which handles ⁴⁵⁹ the digital analysis. The signal can either be processed immediately (in real time) or ⁴⁶⁰ it can be saved to a data storage for analysis at a later stage (offline). The devices ⁴⁶¹ carrying out the processing can be multipurpose (e.g. Field Programmable Gate ⁴⁶² Arrays) or dedicated (e.g. Application-Specific Integrated Circuits).

⁴⁶³ **Field Programmable Gate Array (FPGA)** is an integrated circuit designed to be ⁴⁶⁴ reprogrammable and reconfigured after manufacturing. It consists of a set of logic ⁴⁶⁵ gates that can be interconnected in numerous combinations to carry out a set of

466 logic operations. Many such logic operations can take place in parallel, making the
467 FPGA a powerful tool for signal processing. FPGAs are often used during system
468 development or in systems in which the requirements might change with time. They
469 can be reprogrammed in the order of seconds. In addition, the logic design only needs
470 minor changes when migrating to a newer version of the FPGA chip of the same
471 vendor. The FPGAs also offer faster time-to-market with comparison to application-
472 specific solutions, which have to be developed. On the other hand, the price per
473 part can be significantly higher than for the application-specific solutions. Also, their
474 other major disadvantages are a high power consumption and a relatively low speed
475 as compared to more application-specific solutions. However, today's solutions are
476 capable of clock speeds higher than 500 MHz. Together with the integrated digital
477 signal processing blocks, embedded processors and other modules, they are already
478 very powerful and versatile. All in all, FPGAs are a good choice for prototyping and
479 limited production, for projects with limited requirements for speed and complexity.

480 **Application-Specific Integrated Circuit** (ASIC) is an integrated circuit designed
481 for a specific use. The design cannot be modified after chip production, as is the case
482 with FPGAs. On the other hand, the ASICs can be optimised to perform a required
483 operation at a high speed and at a low power consumption. In addition, due to the
484 specific design the size of the chip can be much smaller. ASICs can be designed as
485 hybrid chips, containing both a digital and an analog part. Finally, ASICs can be
486 designed to withstand much higher irradiation doses than FPGAs and can therefore
487 be used in harsh environments like in space or in particle colliders.

488 To update the chip, the design has to be submitted to a foundry, which produces
489 the new chips with a turnover time of 4—6 weeks. The costs of a submission start
490 at \$ 50 000, but the price per part can be reduced significantly with a high volume.
491 To sum up, ASICs are used for high volume designs with well defined requirements
492 where some stringent constraints in terms of power consumption and speed have to
493 be met.

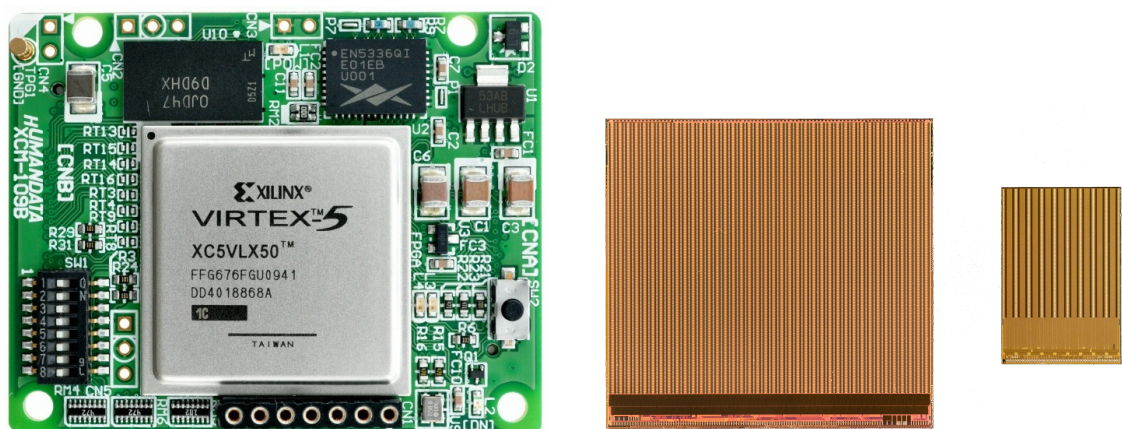


Figure 1.14: An example of a Xilinx Virtex 5 FPGA [1] and an FE-I4 and FE-I3 ASIC chip [3].

⁴⁹⁴ Bibliography

- ⁴⁹⁵ [1] *Xilinx Virtex 5 FPGA*. <http://www.hdl.co.jp/XCM-109/top.560.jpg>.
- ⁴⁹⁶ [2] W. Blum, W. Riegler, and L. Rolandi. Particle Detection with Drift Chambers,
⁴⁹⁷ volume 2 of 2. Springer-Verlag, Berlin Heidelberg, 2008.
- ⁴⁹⁸ [3] M. Garcia-Sciveres. ATLAS Experiment Pixel Detector Upgrades. 2011.
- ⁴⁹⁹ [4] Hendrik Jansen, Daniel Dobos, Thomas Eisel, Heinz Pernegger, Vladimir Eremin,
⁵⁰⁰ and Norbert Wermes. Temperature dependence of charge carrier mobility in
⁵⁰¹ single-crystal chemical vapour deposition diamond. *Journal of Applied Physics*,
⁵⁰² 113(17), 2013.
- ⁵⁰³ [5] S. Ramo. *Currents Induced by Electron Motion*. *Proceedings of the IRE*, 27:584–
⁵⁰⁴ 585, 1939.
- ⁵⁰⁵ [6] W. Shockley. *Currents to Conductors Induced by a Moving Point Charge*. *Journal*
⁵⁰⁶ *of applied Physics*, 9:635, 1938.